

From pseudomorphic to orthomorphic growth of Fe films on Cu₃Au(001).

F. Bruno^a, S. Terreni^b, L. Floreano^a, D. Cvetko^{a,c}, P. Luches^d, L. Mattera^b, A. Morgante^{a,e}, R. Moroni^b, A. Verdini^a, and M. Canepa^{b,*}

^a*Laboratorio TASC dell'Istituto Nazionale per la Fisica della Materia, Trieste, Italy.*

^b*INFN and Dipartimento di Fisica, Università di Genova,
via Dodecaneso 33, I-16146 Genova, Italy*

^c*J. Stefan Institute, University of Ljubljana, Slovenia, and Sincrotrone Trieste, Italy*

^d*INFN and Dipartimento di Fisica, Università di Modena e Reggio Emilia, Modena, Italy.* ^e*Dipartimento di Fisica dell'Università di Trieste, Italy.*

The structure of Fe films grown on the (001) surface of a Cu₃Au single crystal at room temperature has been investigated by means of Grazing Incidence X-Ray Diffraction (GIXRD) and Photo/Auger-Electron Diffraction (ED) as a function of thickness in the 3-36 Å range. The combination of GIXRD and ED allows one to obtain quantitative information on the in-plane spacing *a* from the former technique, and the ratio between the vertical spacing *c* and *a*, from the latter one. At low coverage the film grows pseudomorphic to the face centered cubic substrate. The experimental results obtained on a film of 10 Å thickness clearly indicate the overcoming of the limit for pseudomorphic growth. Above this limit the film is characterized by the coexistence of the pseudomorphic phase with another tetragonally strained phase, which falls on the epitaxial line of ferromagnetic face-centered cubic Fe. Finally, above ~ 17 Å the development of a body-centered phase α , whose unit cell is rotated of 45° with respect to the substrate one, has been clearly observed. α is the dominating phase for film thickness above ~ 25 Å and its lattice constant evolves towards the orthomorphic phase in strict quantitative agreement with epitaxial curves calculated for body centered tetragonal iron phases.

PACS: 68.55.-a; 68.55.Jk; 61.14.Qp

* Corresponding author: Tel: **39-010-3536287; Fax: **39-010-311066;

E-mail address: canepa@fisica.unige.it; www.fisica.unige.it/surfmag

INTRODUCTION

Very thin iron films, with physical properties at variance with the ordinary α -Fe phase, can be grown on appropriately chosen substrates.¹ Such "artificial" phases represent an ideal ground in the investigation of the interplay between the structure and the magnetic properties of materials.² In this field, the $\text{Cu}_3\text{Au}(001)$ surface has been considered as a candidate for the stabilisation of a face-centered-cubic (fcc), expanded volume, high-spin Fe phase.³ For this substrate, a model of the so-called epitaxial lines of iron, calculated within the frame of linear elasticity theory, suggested the formation of a tetragonally strained phase, with some uncertainty on its body or face centered geometry.⁴ The calculations did not consider interdiffusion processes between the Fe deposit and surface atoms, but both intermixing at the interface and substrate segregation have been reported for Fe deposited at room temperature (RT) on $\text{Cu}(001)$ ⁵ and on $\text{Au}(001)$.^{6,7}

In previous research on the magnetism of the $\text{Fe}/\text{Cu}_3\text{Au}(001)$ films, three regions of thickness of different properties were identified.⁸⁻¹⁰ At sub-monolayer coverage no hysteresis loops were detected. A second region was instead characterised by a magnetisation perpendicular to the surface. Then, at a critical thickness Θ_{sw} of the order of a few monolayers and depending on the temperature of deposition, the magnetisation was found to switch to an in plane orientation (spin reorientation transition, in brief SRO) as in ordinary α -Fe.

In spite of an overall agreement on film magnetism, no general consensus has been reached about the film structure. Regarding room temperature (RT) growth, an early LEED study claimed the occurrence of a face-centered cubic phase up to 7 Mono-Layers (ML).⁸ In a more recent LEED I-V investigation the SRO transition ($\Theta_{sw} \sim 4$ ML) was tightly related to a transition from an fcc to a bcc-like phase;⁹ the LEED analysis was successively backed by an STM study in the coverage range of the SRO transition, pointing out a complex topography assigned to the coexistence of different phases.¹¹ Another LEED I-V study, backed by dynamical calculations, proposed instead a body-centered-tetragonal (bct) structure down to $\Theta = 3.3$ ML with no apparent correlation between structural properties and the SRO transition.¹² In fact, the latter experiments must be carefully taken into consideration, since they were performed on substrates prepared by pre-depositing 2 ML of Fe at 150 K. For this temperature and thickness range, we have recently shown that the structure and morphology of the growing film is driven by electronic mechanisms,¹³ whereas only strain and thermally activated processes drive the RT growth. Finally, in a recent electron scattering experiment (in the so-called Primary-beam Diffraction Modulated Electron Emission configuration, PDME)¹⁴ an fcc-like structure was found for $\Theta < 4$ ML; then in a region extending up to

≈ 23 ML, two different phases were detected. A unique phase of bct type was finally detected, at least within the outermost layers, for relatively thicker films, in agreement with results of Ref.¹² Ref.¹⁴ considered atomic exchange processes in some details, indicating the occurrence of a limited Au intermixing and segregation at the initial stages of growth.

The somewhat conflicting results demand for further investigation. Here we report on experiments of $\text{Fe}/\text{Cu}_3\text{Au}(001)$ RT growth performed at the ALOISA beamline at the Elettra Synchrotron (Trieste, Italy).¹⁵ Our investigation deals with a structural characterization of films in a thickness range of 3-36 Å, performed by means of X-ray induced photo- (and/or Auger-) electron Diffraction (from now on ED for brevity) in the so-called forward scattering condition. In this condition, the emission intensity is enhanced along the direction of interatomic axes by means of a focusing effect.¹⁶ The angular position of focusing peaks in polar ED scans is well known to provide "simple", chemically selected, short range information on the structure of the topmost layers of the films.^{17,18} Furthermore, the availability of reliable calculations codes allows for a close comparison with experimental data and for quantitative analysis.¹⁹

In our experimental approach,²⁰ ED data are backed by Grazing Incidence X-Rays Diffraction (GIXRD) measurements, supplying information about the in-plane lattice parameter of films²¹ and about the film morphology. In the next section details on the experimental procedures are reported. Experimental data will be described in sect. II. A quantitative analysis of the data can be found in the sect. III. A discussion of the results obtained follows in sect. IV. A summary and the conclusions can be found in sect. V.

I. EXPERIMENTAL

The beamline ALOISA allows users to perform both electron spectroscopy and X-Ray surface diffraction measurements under the same experimental conditions.^{15,22} The sample is mounted on a 6-degrees-of-freedom manipulator, specially designed to select with great accuracy (0.01°) the grazing angle of the beam electric field. The temperature of the sample, measured by thermocouples, can be varied by resistive heating and liquid nitrogen cooling. The UHV experimental chamber (base pressure in the 10^{-11} mBar range) hosts the hemispherical electron analysers and X-Ray detectors. The emission direction from the sample surface can be freely selected for any orientation of the surface. For the surface preparation, the sample is translated in the preparation chamber (base pressure of $1 - 2 \times 10^{-10}$ mBar) equipped with facilities for sputtering, evaporation cells, gas inlets and a RHEED system.

The surface preparation procedure was set up in previous He diffraction experiments.^{23,24} The procedure

takes into account the particular thermodynamics of Cu₃Au(001), that is characterized by a continuous order/disorder (O/D) phase transition at the surface with a critical temperature T_c = 663 K²⁴ and a bulk first order O/D transition at the same T_c.²⁵ An ordered surface, displaying sharp *c*(2 × 2) RHEED patterns typical of the Au-Cu termination,²⁶ was obtained by sputtering and careful annealing procedures described in details elsewhere.²⁴ The same sample was also used in a previous synchrotron experiment²⁰ and in the PDMEE experiment of Ref.¹⁴.

At ALOISA, XPS surveys at grazing incidence (of the order of the critical angle) were used to check contamination of light adsorbates and Fe residuals after the sputtering removal of films. A preliminary ED characterization of the substrate, backed by multiple scattering calculations has been presented in a previous paper.²⁰ Simulations taking into account the geometry for the Au-Cu termination available in literature²⁷ were found to be in excellent agreement with experimental results.

Iron was evaporated from a carefully outgassed electron bombardment cell (Omicron). A quartz microbalance allowed to tune the deposition flux (typically of the order of 1 layer per minute) prior to the deposition on the sample. In the series of experiments presented in this paper, the film thickness was calibrated by X-ray reflectivity from the sample during and after deposition. Fig. 1 shows a typical deposition curve, measured at an incidence (tilt) angle $\alpha_{in} = 8.25^\circ$ and a photon energy of 3500 eV during film deposition at room temperature. The interference between the waves reflected by the film-vacuum and the substrate-film interfaces yields an oscillatory evolution of the reflectivity as a function of the overlayer thickness. For the selected vertical momentum transfer $k_z = 2\frac{E}{\hbar c} \sin \alpha_{in}$, identical phase conditions occur after a thickness increase of $\Delta D = \frac{2\pi}{k_z} = 12.35 \text{ \AA}$, thus leading to an accurate calibration of the deposition rate. In the sequence of experiments, Fe evaporation was stopped at different points of the deposition curve ensuring a high reproducibility of the amount of deposited material and a reliable estimate of the coverage.

The post growth GIXRD measurements basically consisted of radial scans along the (200) position in the in-plane Cu₃Au(001) reciprocal lattice. These measurements were run scanning the photon energy in broad ranges under a suitable θ - 2θ scattering geometry. Both the incidence angle of the beam and the emission angle were kept below the experimentally determined critical angle. The observation of diffraction peaks in radial scans allows to determine the in-plane spacing d through the Bragg condition $2d \sin \theta = hc/E$. Rocking curves of selected Bragg peaks, obtained by rotating the azimuthal angle at fixed energy, were measured to get additional information on the surface morphology.

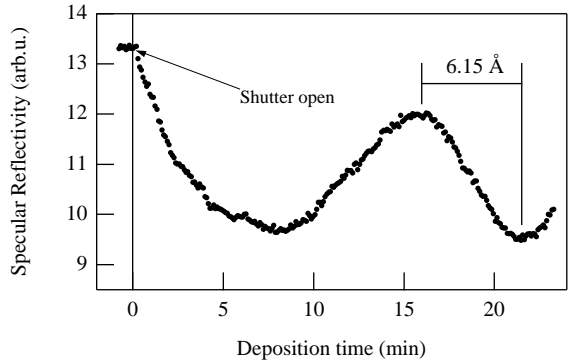


FIG. 1. X-Ray Specular Reflectivity taken during deposition at fixed energy (3500 eV) and grazing angle (8.25°). Maxima and minima arise from the interference between the interface and the growing film surface.

A coverage estimate obtained by XPS measurements was found consistent with the reflectivity measurements within $\pm 20\%$. ED polar scans were measured by rotating the electron analyser in the plane defined by the surface normal and the beam axis, while keeping the grazing angle, the surface azimuthal orientation with respect to the beam axis and the polarization orientation fixed. We considered emission along $\langle 100 \rangle_{sub}$ and $\langle 110 \rangle_{sub}$, the two main symmetry direction of the surface cell of the substrate. The photon energy was set to about 900 eV in order to look at several photoelectron and Auger peaks of Fe, Cu and Au. Here we will focus on the Fe L_{2,3}M₂₃M₄₅ line at a K. E. of 698 eV. The signal was collected at the maximum and at suitably chosen energies aside the peak, in order to allow an effective subtraction of the background of secondaries.

II. RESULTS

A. GIXRD

In fig. 2, (H,0,0) radial scans taken on films of different thickness are shown. The pattern measured on the bare substrate is reported for comparison. In the measurements of fig. 2 the photon beam impinges the surface at grazing incidence, forming an angle $\theta = 45^\circ$ with respect to the fcc(100) planes of the direct lattice.

Only a slight broadening of the (200)_{sub} peak of the substrate was observed at low coverage. A weak but fully detectable Fe-induced peak, indicated with α' in fig. 2, was detected at $\sim 10 \text{ \AA}$, marking the first structural (and morphological) transition. The peak α' becomes more intense in the 10-17 \AA range. A shoulder appears at the left hand side of peak α' at $\Theta > 17 \text{ \AA}$. For $\Theta \geq 25 \text{ \AA}$ this shoulder develops in the well defined peak α , that gradually moves away from the (200) reflection.

The position of the α' peak in the 10 \AA pattern of fig. 2, 1.93 ± 0.005 r.l.u., corresponds to a distance d_{100}

$=1.94 \pm 0.01 \text{ \AA}$ along the $\langle 001 \rangle$ direction of direct space, eventually leading to a square cell of side $a_{\alpha'} = d \cdot \sqrt{2} = 2.74 \pm 0.01 \text{ \AA}$. This value can be compared with the lattice parameter of $\text{Cu}_3\text{Au}(001)$ ($a_{\text{CuAu}} = 2.65 \text{ \AA}$), with an estimate of $a_{\text{fcc}} \sim 2.55 \text{ \AA}$ for an hypothetical fcc iron structure⁴, and with $a_{\text{bcc}} = 2.87 \text{ \AA}$, e.g. the lattice parameter of a bcc film whose unit cell is rotated of 45° with respect to the fcc substrate (hereafter indicated as $R^{45}\text{bcc}$).

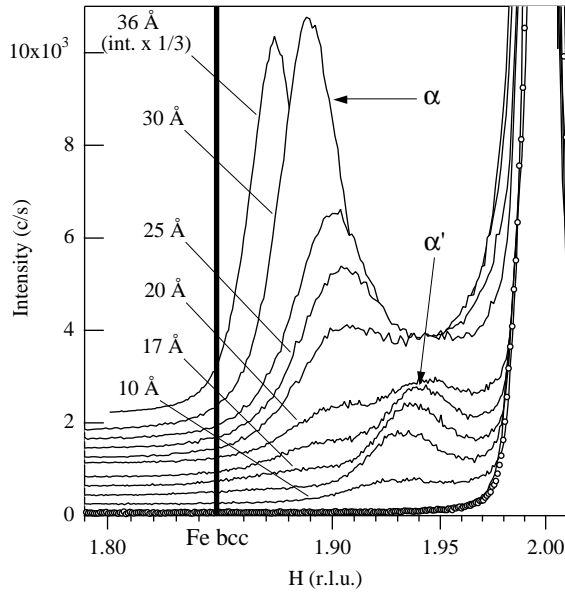


FIG. 2. In plane X-Ray Diffraction of the $(2,0,0)$ diffraction peak taken at fixed scattering geometry by varying the photon energy. The data are shown as a function of the reciprocal lattice unit H of the fcc $\text{Cu}_3\text{Au}(100)$ substrate. Diffraction from the clean substrate is shown with open markers. Full lines are the diffraction measurements from Fe films at different thickness. The data have been vertically shifted by a constant offset (200 c/s) for the sake of clarity.

The position of the α peak at 36 \AA thickness in Fig. 2 corresponds to a lattice parameter $a_{\alpha} = 2.830 \pm 0.005 \text{ \AA}$. The position of α is indeed close to the (110) reflection of a $R^{45}\text{bcc}$ structure. Further, reasonable arguments on the energetics of iron modifications and inspection of the so-called epitaxial lines calculated in Ref.⁴ led to consider the α peak incompatible with an fcc-like modification (fct phase). The α peaks were therefore assigned to tetragonally strained body centered ($R^{45}\text{bcc}$) structures.

The GIXRD measurements provided therefore valuable insight on the in-plane structure of the films; this information is relatively direct for those patterns presenting one dominant Fe-induced peak, as it is the case at very low (10 \AA) and very large coverages (36 \AA). In an intermediate region between 10 and 20 \AA , the patterns are more complex, likely reflecting the coexistence of more than one phase in the film. A full structural determination requires also the value of the vertical lattice

constant of the various iron phases which forms at different thickness. We extracted this information by ED, in the forward focusing regime.

B. ED

ED polar scan measured on film of selected thickness for the Fe Auger line along the $\langle 100 \rangle_{\text{sub}}$ and $\langle 110 \rangle_{\text{sub}}$ directions, are reported in Figs. 3 and 4, respectively. The patterns were obtained after subtraction of the background of secondaries. The peak F is originated by the forward scattering effect along off-normal nearest-neighbour chains. The position of this peak provides a guess on the ratio between the in-plane and vertical lattice constants of the film. In this respect, dotted and dashed lines in Figs. 3 and 4 mark the position of the F peak expected in case of fcc and $R^{45}\text{bcc}$ geometry, respectively.

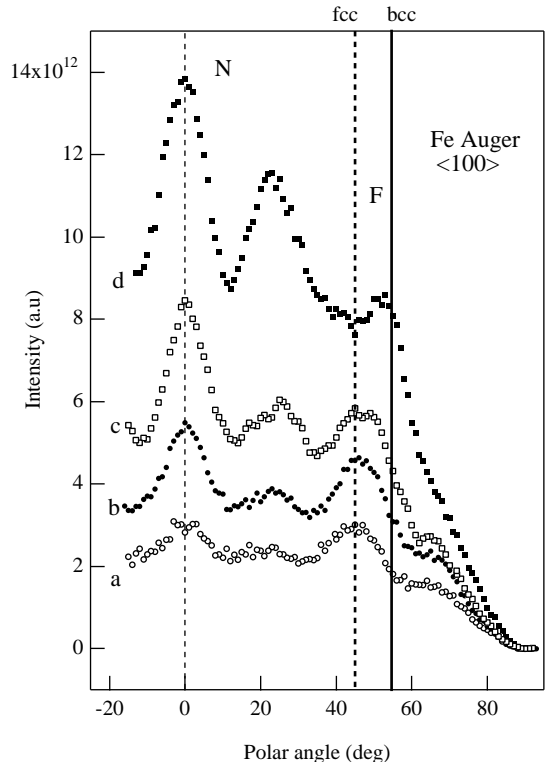


FIG. 3. Experimental Fe Auger LMM (K.E. = 698 eV) ED pattern along $\langle 100 \rangle$ substrate symmetry direction for: a) the 3 \AA film, b) the 10 \AA film, c) the 20 \AA film, d) the 36 \AA film. The surface normal direction (N) and the first neighbor direction (F) are also indicated.

At the lowest coverage investigated (patterns *a* of Figs. 3 and 4), the forward focusing peak F is fairly pronounced in the $\langle 100 \rangle_{\text{sub}}$ scan close to the fcc-like position. The F peak lies close to the fcc marker in the $\langle 110 \rangle_{\text{sub}}$ direction as well, though its intensity is very weak. Note in both patterns the presence of the forward focusing peak N ,

related to close-packed chains along the surface normal. At 10 Å (pattern *b* of Figs. 3 and 4) the F peaks move slightly from the fcc markers towards larger polar angles. The angular shift of the F peaks becomes more evident at $\Theta = 20$ Å (patterns *c*). Also the shape of the patterns shows evident variations with respect to lower coverages. In the spectra obtained on the film at $\Theta = 36$ Å (patterns *d*), the F peak becomes narrower and shifts decisively towards the bcc position.

We performed also ED measurements for the Auger lines of Cu and for the Au 4f_{7/2} photoemission line. The experimental data resulted in overall agreement with results of Ref.¹⁴, obtained on the same sample and under similar experimental conditions of this paper. We address the reader to Ref.¹⁴ for a careful discussion of the intermixing between iron and substrate species.

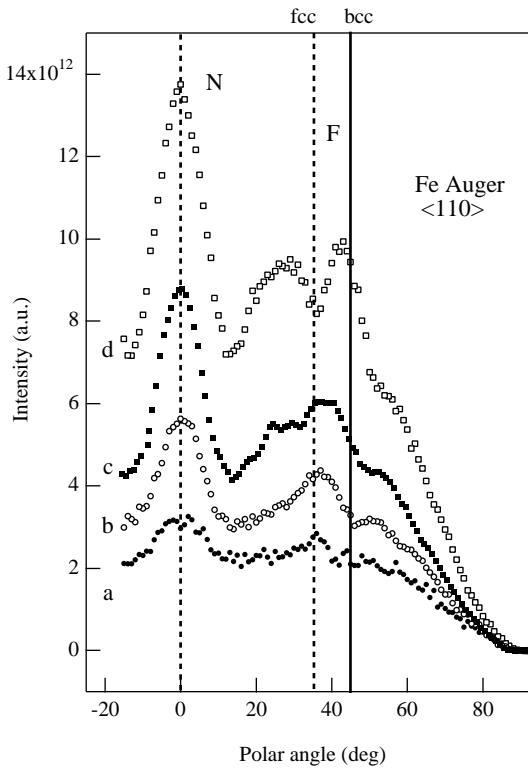


FIG. 4. Same of Fig. 3, but for the $\langle 110 \rangle$ substrate symmetry direction. a) The 3 Å film, b) the 10 Å film, c) the 20 Å film, d) the 36 Å film.

III. ED DATA ANALYSIS

In this section we present the structural models for the Fe film at different thickness, as obtained by comparison of the ED experimental data to multiple scattering calculations. In our computational approach the ED polar pattern $I_{exp}(\theta)$ is considered as a superposition of two contributions, according to the expression:

$$I_{exp}(\theta) = ISO_{exp}(\theta) \cdot (1 + \chi_{exp}(\theta)) \quad (1)$$

where $ISO_{exp}(\theta)$ is a smooth, nearly isotropic background and the anisotropy term $\chi_{exp}(\theta)$ is the diffractive part of the pattern, carrying the information on the interatomic distances.

The ISO_{exp} contribution is generally obtained by interpolating $I_{exp}(\theta)$ to a polynomial and divided out in order to extract χ_{exp} , which is then compared to calculated $\chi_{calc}(\theta)$ ²⁸. We have preferred to afford a calculation of the ISO term. Thus, the polar scans $I_{exp}(\theta)$ have been compared with calculations:

$$I_{calc}(\theta) = ISO_{calc}(\theta) \cdot (1 + \chi_{calc}(\theta)) \quad (2)$$

For any given model the anisotropy term χ_{calc} has been calculated by means of the MSCD code package²⁹, while the ISO term has been written as the product of several factors.^{30,31} First, an emission factor accounts for the electron emission matrix element;³² it is determined by the polarization of the beam and by the initial and final states of the emitted electron. A second factor bears the information on the excited electron escape path through the Fe film;³⁰ it depends on the thickness and the homogeneity of the film. A third factor accounts for the surface roughness.³³ Finally, an instrumental factor accounts for the beam spot size on the sample and the angular acceptance of the detector. The calculation of the ISO part requires therefore reasonable estimates on the thickness and the surface roughness of the film and on the electronic mean free path.

Concerning MSCD calculations, the non structural input parameters, i.e. Multiple Scattering order = 6 and the inner potential = 10 eV have been fixed for all the simulations. Clusters of at least 180 atoms have been considered. The isotropic emission for the Auger electrons has been simulated by the transition from an initial p-level to an s (*l*-1) final-state level.

The value of the lattice parameter of the in-plane square cell *a* has been obtained from the GIXRD measurement, while the ratio between the vertical spacing *c* and *a*, was first estimated by visual inspection of the angular position of the F peaks in the ED patterns. With these input parameters, the structural models have been refined by calculating $\chi_{calc}(\theta)$ as a function of *a* and *c*.

A. Low Coverage: $\Theta < 10$ Å

The patterns of Figs. 3 and 4 force to consider an fcc-like structure. Although results from Ref.^{14,20} suggested a limited degree of mixing of Au in the first few layers, a reasonable fitting of the data was possible disregarding atomic exchange processes.³⁴ The comparison between MSCD calculations and the experimental ED scans is reported in fig. 5. Note that the same $ISO_{calc}(\theta)$ is used in both azimuthal directions.

The polar scans compare rather well (dashed lines) with a simple three-layer Fe pseudomorphic fcc film (*a*= 2.65 Å; *c/a* = 1.41) built on an unrelaxed substrate

extending three layers beneath. However, a slightly better agreement (full lines in Fig. 5) was found by admitting a slight tetragonal distortion with $a_\gamma = 2.65 \text{ \AA}$ and $c/a_\gamma = 1.38$.

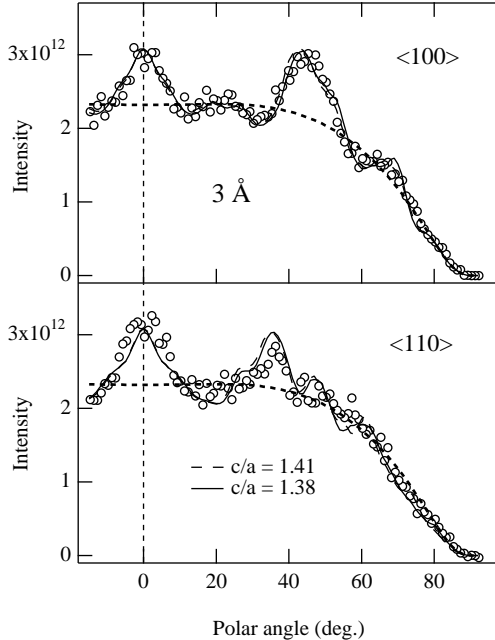


FIG. 5. Comparison of the ED data at 3 \AA Fe thickness with a pseudomorphic model structure. Calculations are shown for both the unrelaxed ($c/a_\gamma = 1.41$, dashed line) and relaxed γ phase ($c/a_\gamma = 1.38$, full line). The same ISO_{calc} component, shown by heavy dashed lines, is used for both azimuthal directions

B. Medium Coverage: $10 \text{ \AA} \leq \Theta \leq 20 \text{ \AA}$

The α' peak in the GIXRD patterns at $\Theta = 10 \text{ \AA}$ indicates a change of the growth mode. GIXRD and ED evidences can be rationalized if the coexistence of the two phases is assumed: the majority fcc-like phase, as seen at low coverage, is accompanied by the nucleation of a new phase α' , minority phase at this stage.

The ED patterns have been compared to calculations performed on a crude model assuming the linear combination of two "independent" phases:

$$I_{th} = A \cdot I_\gamma + B \cdot I_{\alpha'}, \quad (3)$$

where

$$I_\gamma \rightarrow a_\gamma = 2.65 \text{ \AA} \text{ and } c/a_\gamma \sim 1.38$$

$I_{\alpha'} \rightarrow a_{\alpha'} = 2.74 \text{ \AA}$ (from GIXRD) and $c/a_{\alpha'}$ to be determined.

$c/a_{\alpha'}$, A and B were varied in order to find the best agreement with experimental data. Taking into account the estimated thickness of the film, we have modelled a film of about 5-6 layers. A good agreement was obtained

with $c/a_{\alpha'} = 1.22$, $A = 0.6$ and $B = 0.4$ for both azimuthal directions (Fig. 6).

For comparison, we also calculated the simulation for a homogeneous iron phase made of six complete layers, assuming the c/a ratio of 1.32 estimated by simple inspection of the angular position of the maximum of the F peak in the polar pattern. This model yields a simulation of the ED data (not shown) definitely worse than the mixed phases model.

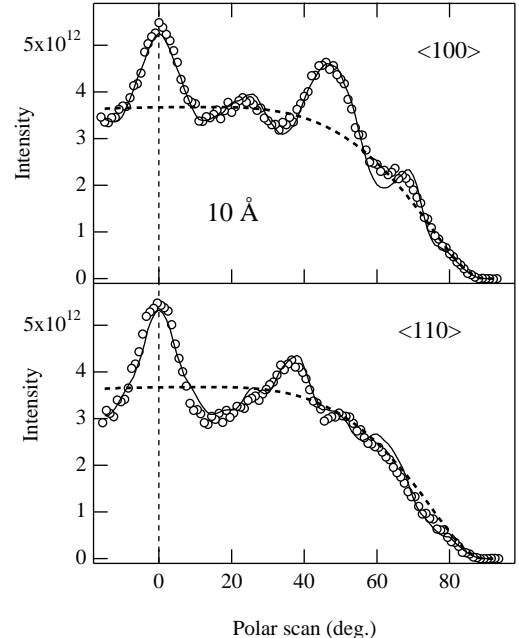


FIG. 6. Comparison of the ED data at 10 \AA Fe thickness with calculations (full lines) based on a model which combines the γ and α' phases. See text for the values of the lattice parameters and the weight of the phases. The same ISO_{calc} component, shown by heavy dashed lines, is used for both azimuthal directions

At 20 \AA the F peaks are clearly shifted, indicating a change of the c/a ratio. Backed by GIXRD, a model considering the superposition of three phases was attempted:

$$I_{th} = A \cdot I_\gamma + B \cdot I_{\alpha'} + C \cdot I_\alpha \quad (4)$$

For simplicity, the parameters for the γ phase and the α' phases were fixed at the same values found at lower coverage:

$$I_\gamma \rightarrow a_\gamma = 2.65 \text{ \AA}, c/a_\gamma \sim 1.38$$

$$I_{\alpha'} \rightarrow a_{\alpha'} = 2.74 \text{ \AA}, c/a_{\alpha'} = 1.22.$$

By taking $A = 0.4$, $B = 0.4$ and $C = 0.2$, a rather satisfactory agreement was found (fig. 7) with the following set of parameters for the phase α ,

$$I_\alpha \rightarrow a_\alpha = 2.80 \text{ \AA}, c/a_\alpha = 1.05.$$

We note that a reasonable agreement was found also with a linear combination of the γ phase ($a_\gamma = 2.65 \text{ \AA}$, $c/a_\gamma \sim 1.38$) and the α' phase ($a_{\alpha'} = 2.74 \text{ \AA}$, $c/a = 1.22$) found at 10 \AA . However, in this case, we have found

rather different values of the A and B coefficients along the two azimuthal directions considered. Finally, the simulation for a homogeneous phase model assuming $c/a = 1.25$, corresponding to the angular position of the F peak in the polar scan, gave a bad quality fit.

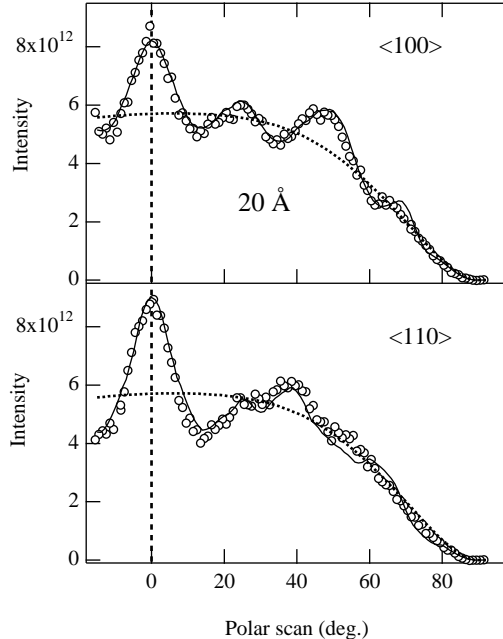


FIG. 7. Comparison of the ED data at 20 Å Fe thickness with calculations (full lines) based on a model which combines three phases (γ , α' and α). See text for the values of the lattice parameters and the weight of the phases. The same ISO_{calc} component, shown by heavy dashed lines, is used for both azimuthal directions.

C. High Coverage: $\Theta > 25$ Å

The in-plane lattice parameter of the α phase at 36 Å determined by GIXRD is $a_\alpha = 2.830 \pm 0.005$ Å. The value of c/a_α was determined by simulation of scattering from a free standing film consisting of a unique phase of 10 layers. The best fit yielded $a_\alpha = 2.83$ Å and $c/a_\alpha = 1.03 \pm 0.02$. The best fit curves along $\langle 100 \rangle_{sub}$ and $\langle 110 \rangle_{sub}$ are reported (full lines) in Fig. 8. We found an excellent agreement along the $\langle 100 \rangle_{sub}$ direction. The simulation reproduces rather accurately the angular position, intensity and width of the N and F peaks. The experimental data are not reproduced equally well along the $\langle 110 \rangle_{sub}$ direction, possibly due to some morphological effect.³⁵ A similar analysis, performed on the film of 30 Å thickness provided $a_\alpha = 2.810 \pm 0.005$ Å and $c/a_\alpha = 1.05 \pm 0.02$.

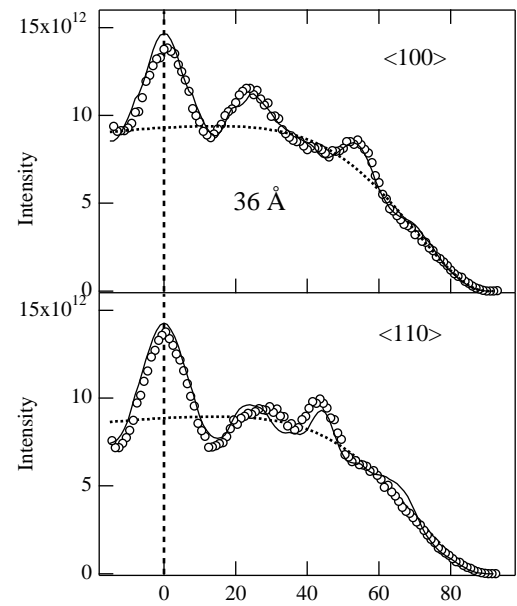


FIG. 8. Fits to the ED data at 36 Å Fe thickness with a body centered tetragonal model structure. The best fit (full lines) was obtained for $a_\alpha = 2.83$ Å and $c/a_\alpha = 1.03$. The same ISO_{calc} component, shown by heavy dashed lines, is used for both azimuthal directions.

IV. DISCUSSION

In Fig. 9, we report the comparison of our results and the other experimental data available in literature with the theoretical prediction for the structure of the bct and fct phases, the so called epitaxial curves⁴ (i.e. the curves where the Poisson ratio between the elastic constants for the given structure is conserved).

The single phase we found at the lower coverage represents the pseudomorphic γ -phase predicted at initial stages of metal-on-metal epitaxy.³⁶ The occurrence of a pseudomorphic γ -phase at low coverage is also reported by other measurements on $\text{Cu}_3\text{Au}(001)$ ^{9,14} and $\text{Cu}_{90}\text{Au}_{10}(001)$.³⁷ As can be seen, the structure of the γ -phase lies above the FM fcc epitaxial line and is locked by the substrate for several layers before the appearance of the α' -phase at ~ 10 Å (for the pseudomorphic phase this corresponds to 5-6 ML). This limit for pseudomorphic growth, marked by the appearance of the peak α' in GIXRD measurements, compares well with the value obtained by a previous LEED I-V study.⁸

A relevant exception to such general agreement on initial stages of growth, is provided by the accurate analysis of Wuttig and coworkers.^{10,12} As can be seen in Fig. 9, the films were found to lie on the bcc epitaxial line already at the coverage of 3.3 ML (i.e. ~ 5 Å, according

to the data in table I of Ref.¹²). This discrepancy could be possibly attributed to the different procedure for film deposition, since the authors of Ref.¹² deposited the first two monolayers at 150 K, while subsequent layers were deposited at 300 K. This procedure is expected to reduce both intermixing and surface segregation. In fact, a fraction of the order of 10% of a monolayer of Au atoms has been found to segregate for $\Theta < 4$ ML upon deposition at RT¹⁴ and a few percents has been found within the Fe film^{8,12,14}. We may speculate that Au and Cu impurities are concurrent in the stabilization of the pseudomorphic γ -phase. The morphology of the growing film is also affected by the deposition procedure. In fact, we previously found by He atom scattering that deposition of 1 layer equivalent at 150 K and subsequent annealing at 400 K yields the formation of an homogeneous pattern of three-layer height islands,¹³ whereas a much higher filling of the first layer (68 %) is obtained upon deposition of 1 ML at RT.¹¹

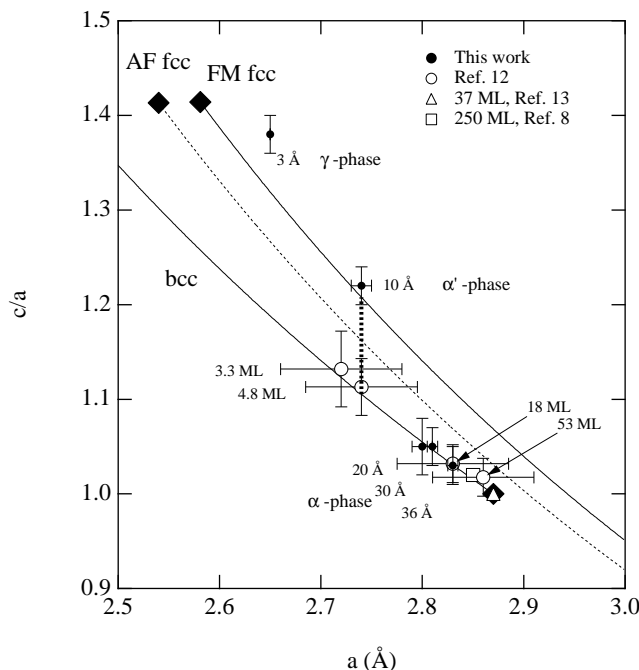


FIG. 9. Comparison of our results and other experimental data available in literature for thick films with the theoretical prediction for the structure of the bct [after Ref. 4] and fct [after Ref. 12] phases, the so called epitaxial curves (full and dashed lines). The full circles represent our structural determinations. The open circles represent the determinations of Ref. [12]. The open triangle and the open square represent the measurement of Ref. [13] at 37 ML and that of Ref. [8] for a 250 ML film, respectively. The path for the transition from the fct to bct phase is indicated by the heavy dotted line.

Whatever the effect of temperature on segregation, structure and morphology, our measurements do not support a direct relation between the SRO transition and the fct to bct one. In fact, the latter phase only appears at a thickness larger than 17 Å, i.e. well beyond the

2.5-3.5 ML range claimed in the literature for the SRO transition.^{8,10,9} On the basis of the present data, we cannot exclude a connection between the transition from the pseudomorphic γ -phase to the fct α' -phase and the SRO transition.

The film evolution in the 10-20 Å coverage range is the most interesting one since up to three different phases are seen to co-exist. The α' phase is seen to nicely fit the epitaxial line for FM fcc Fe. Its lattice parameter at 10 Å, $a_{\alpha'} = 2.74 \pm 0.01$ Å, seems to be the maximum allowed strain for this fct phase; in fact, when the third phase α appears at higher coverage, $a_{\alpha'}$ rather shrinks (see Fig. 2). This indicates that the appearance of the α phase partially relieves the strain of the fct film. The α phase, when appearing above 17 Å, has already a lateral lattice spacing of 2.80 Å, which, together with the vertical spacing determined by MSCD analysis, brings the new phase directly on the bcc epitaxial line. No diffraction features are observed for lateral lattice spacings ranging from 2.74 Å up to 2.80 Å. Upon further deposition, the "asymptotic" orthomorphous α phase evolves along the bcc epitaxial line. The structure of this phase is seen to be fully consistent with previous data reported in the literature for thick films.^{8,12,14,8} From our data, the transition path between the fct and bct structure can be traced at the value of maximum tensile strain $a_{\alpha'} = 2.74$ of the α' phase. The observation of a bct phase with the same lateral lattice constant was not possible, in fact the appearance of the α phase is accompanied by a partial relief of strain as witnessed by the slight decrease of $a_{\alpha'}$. On the other hand, the limit value for the bct stability was apparently reached by the group of Wuttig.¹² By following a different preparation procedure, they stabilized the bct phase down to four monolayers, with a corresponding lateral lattice constant in excellent agreement with the 2.74 Å value, we found for the limit of stability of the fct phase (see Fig. 9).

It is interesting to compare this system with the Fe/Cu(100) one. In the latter case, Fe is also seen to grow with an fcc pseudomorphic structure for at least 4 ML, at higher coverage the magnetic properties change and the formation of buffer layers with anti-ferromagnetic fcc structure is proposed. An fcc(100) to bcc(110) transition takes place at about 10 ML, (which is also accompanied by an SRO transition) but, in this case, the whole film is observed to deconstruct, i.e. a martensitic phase transition takes place.^{38,39} This is not observed for Fe on Cu₃Au(001), where the α' phase is still detectable beyond a thickness of 20 Å. In any case the formation of the bct phase is accompanied by a significant amount of surface roughness, possibly leading to the exposure of the layers closer to the Fe/substrate interface (which are still probed by PED at 20 Å, see section III.B). This is consistent with a quantitative evaluation of the bct domain size obtained by the width of the diffracted α peaks. The profiles of the R^{45} bct (110) and R^{45} bct (100) peaks, obtained with an azimuthal scan at fixed photon energy (not shown), yielded a mean domain size of ~ 150 Å for

the 36 Å film thickness. This high level of morphological disorder is consistent with the experimental findings for homoepitaxial deposition of Fe on Fe(001) at RT, where, in absence of surfactant species, the growth is seen to proceed in a three-dimensional fashion,^{40,41} resulting in the formation of pyramidal mound-like structures.⁴²

V. CONCLUSIONS

We have presented a combined GIXRD-ED study of the growth of thin films of Fe on Cu₃Au(001). We observed the formation of different phases as a function of the film thickness. The main conclusions of this investigation can be summarized as follows:

i. A single pseudomorphic phase of nearly fcc character (γ -phase) was observed below 10 Å thickness. This conclusion is consistent with most of the previous works in literature^{3,8,9,14} whereas it seems in apparent contrast with the analysis of Ref.¹² that reports a bct phase down to \sim 5 Å. In this respect, we suggested that exchange processes at the interface¹⁴ can concur to the stabilization of the γ phase and we speculate that the different results of Ref.¹² are due to a lower influence of intermixing obtained during the deposition of the first two layers at 150 K.

ii. On a 10 Å thickness film, a neat Fe induced peak, clearly illustrating the overcoming of the thickness limit for pseudomorphic growth, has been observed from the in-plane GIXRD measurements. Above this limit the film is characterized by the coexistence of phases: the γ -like pseudomorphic phase, most likely in inner layers, and a second strained phase α' . The latter phase is seen to lie on the ferromagnetic fcc epitaxial line.

iii. Above 17 Å, we clearly observed the nucleation of a third strained phase, α , which becomes the dominating structure above 25 Å. The α phase is characterized by a body centered, tetragonally strained structure, whose unit cell is rotated of 45° with respect to the fcc substrate. The strain is progressively relieved with the increasing film thickness, in close agreement with the results of Ref.¹². The experimentally determined lattice constants of α are in strict quantitative agreement with the epitaxial curves for bcc Fe.

ACKNOWLEDGEMENTS

Maurizio Canepa, Silvana Terreni and Lorenzo Matta are very grateful to Fernando Tommasini for his continuous support to this experiment. The authors are then grateful to P. Cantini, G. Boato, S. Valeri and A. Di Bona for stimulating discussions on the Fe/Cu₃Au system. The authors thank G. Gazzadi for discussions on the MSCD calculations and C. Mannori, S. Prandi and

M. Repetto for helpful assistance at various stages of the experiment.

Funding from INFM and from the Italian Ministero dell'Università e Ricerca Scientifica (Cofin 990211848) are gratefully acknowledged.

¹ M. Wuttig, B. Feldmann and T. Flores, *Surf. Sci.* **331-333**, 659 (1995).

² V.L. Moruzzi, P.M. Marcus, and J. Kübler, *Phys. Rev. B* **39**, 6957 (1989); P.M. Marcus, V.L. Moruzzi and S.-Q. Qiu, *Phys. Rev. B* **60**, 369 (1999).

³ S.H. Lu, J. Quinn, D. Tian, F. Jona and P.M. Marcus, *Surf. Sci.* **209**, 364 (1989).

⁴ P.M. Marcus and F. Jona, *Surf. Rev. and Lett.* **1**, 15 (1994).

⁵ D.D. Chambliss, R.J. Wilson and S. Chiang, *J. Vac. Sci. Technol. A* **10**, (1992) 1993; M.T. Kief and W.F. Egelhoff, *Phys. Rev. B* **47**, 10785 (1993).

⁶ R. Opitz, S. Löbus, A. Thissen and R. Courths, *Surf. Sci.* **370**, 293 (1997).

⁷ O.S. Hernan, A.L. Vazquez de Parga, J.M. Gallego and R. Miranda, *Surf. Sci.* **415**, 106 (1998).

⁸ R. Rochow, C. Carbone, Th. Dodt, F.P. Johnen and E. Kisker, *Phys. Rev. B* **41**, 3426 (1990).

⁹ M.-T. Lin, J. Shen, W. Kuch, H. Jenniches, M. Klaua, C.M. Schneider and J. Kirschner, *Phys. Rev. B* **55**, 5886 (1997).

¹⁰ B. Feldmann, B. Schirmer, A. Sokoll and M. Wuttig, *Phys. Rev. B* **57**, 1014 (1998).

¹¹ M.-T. Lin, J. Shen, W. Kuch, H. Jenniches, M. Klaua, C.M. Schneider and J. Kirschner, *Surf. Sci.* **410** 298 (1998).

¹² B. Schirmer, B. Feldmann and M. Wuttig, *Phys. Rev. B* **58** 4984 (1998).

¹³ M. Canepa, P. Cantini, C. Mannori, S. Terreni and L. Mattera, *Phys. Rev. B* **62**, 13121 (2000).

¹⁴ P. Luches, A. Di Bona, S. Valeri and M. Canepa, *Surf. Sci.* **471**, 32 (2000).

¹⁵ An updated presentation of the beamline can be found at <http://tasc.area.trieste.it/tasc/lds/aloisia/aloisia.html>.

¹⁶ S. Kono, S.M. Goldberg, N.F.T. Hall and C.S. Fadley, *Phys. Rev. Lett.* **41**, 1831 (1978).

¹⁷ C.S. Fadley, *The Study of Surface Structures by Photoelectron Diffraction and Auger Electron Diffraction in Synchrotron Radiation research: Advances in Surface and Interface Science, Vol. 1: Techniques*, edited by R. Z. Bachrach, Plenum Press, New York, (1992), and references therein.

¹⁸ W.F. Egelhoff jr. in *Ultrathin Magnetic Structures I*, J.A.C. Bland and B. Heinrich eds., chapt. 5.1, p. 220, Springer - Verlag, Berlin 1994.

¹⁹ Y. Chen, F.J. Garcia de Abajo, A. Chassé, R.X. Ynzunza, A.P. Kaduwela, M.A. Van Hove and C.S. Fadley *Phys. Rev. B* **58**, 13121 (1998).

²⁰ F. Bruno, D. Cvetko, L. Floreano, R. Gotter, C. Mannori, L. Mattera, R. Moroni, S. Prandi, S. Terreni, A. Verdini and M. Canepa, *Appl. Surf. Sci.* **162-163**, 340 (2000).

²¹ B.M. Lairson, A.P. Payne, S. Brennan, N.M. Rensing, B.J. Daniels and B.M. Clemens, *J. Appl. Phys.* **78**, 4449 (1995).

²² L. Floreano, G. Naletto, D. Cvetko, R. Gotter, M. Malvezzi, L. Marassi, A. Morgante, A. Santaniello, A. Verdini, F. Tommasini and G. Tondello *Rev. of Sci. Inst.* **70**, 3855 (1999).

²³ C. Mannori, T. Scimia, P. Cantini, S. Terreni, M. Canepa and L. Mattera, *Surf. Sci.* **433**, 307 (1999).

²⁴ C. Mannori, G. Boato, M. Canepa, P. Cantini, L. Mattera and S. Terreni, *Europhysics Lett.* **45**, 686 (1999).

²⁵ For a review, see H. Dosch, *Critical Phenomena at surfaces and interfaces*, Springer Tracts Mod. Phys., vol. 126 (Springer, Berlin) 1992.

²⁶ E.G. McRae and R. Malic, *Surf. Sci.* **148**, 551 (1984).

²⁷ W.E. Wallace and G.J. Auckland, *Surf. Sci. Lett.* **275**, L685, (1992).

²⁸ G.C. Gazzadi, P. Luches, A. Di Bona, L. Marassi, L. Pasquali, S. Valeri and S. Nannarone, *Phys. Rev. B* **61**, 2246 (2000).

²⁹ <http://electron.lbl.gov/mscdpack/mscdpack.html>. Further information can be found in *MSCD Package User Guide - Simulation of Photoelectron Diffraction using Rehr-Albers Separable Representation* by Y. Chen, M.A. Van Hove, handled out at *Trieste School on Use of Synchrotron Radiation, November 1997*.

³⁰ C.S. Fadley *Basics Concepts of X-Ray Photoelectron Spectroscopy in Electron Spectroscopy, Theory, Techniques and Applications*, C.R. Brundle and A.D. Baker Eds. (Pergamon Press, 1978), Volume II, Chapter 1.

³¹ F. Bruno, PhD. Thesis, *Growth Methods at ALOISA*, November 2000, University of Trieste.

³² J.W. Cooper, *Phys. Rev. A* **47**, 1841 (1993).

³³ A.V. Yakovenko, *J. Electron Spectroscopy and Relat. Phenom.* **74**, 237 (1995).

³⁴ The substrate temperature proved to be a very critical parameter in determining the level of Au surface segregation. In fact, the higher Au concentration at the Fe film surface, we found in the preliminary experiments [Ref. 20], was associated with a slightly higher (15 -20 °C) substrate temperature during deposition.

³⁵ Y. Park, E. E. Fullerton and S.D. Bader, *Appl. Phys. Lett.* **66**, 2140 (1995).

³⁶ J.H. Van Der Merwe, *J. Appl. Phys.* **34**, 117 (1963).

³⁷ S.S. Kang, W. Kuch and J. Kirschner, *Phys. Rev. B* **63**, 024401 (2000).

³⁸ K. Kalki, D.D. Chambliss, K.E. Johnson, R.J. Wilson and S. Chiang, *Phys. Rev. B* **48**, 18344 (1993); S. Müller, P. Bayer, C. Reischl, K. Heinz, B. Feldmann, H. Zillgen and M. Wuttig, *Phys. Rev. Lett.* **74**, 765 (1995); J. Giergiel, J. Shen, J. Woltersdorf, A. Kirilyuk and J. Kirschner, *Phys. Rev. B* **52**, 8528 (1995).

³⁹ A. Biedermann, M. Schmid and P. Varga, *Phys. Rev. Lett.* **86**, 464 (2001).

⁴⁰ J.A. Stroscio, D.T. Pierce and R.A. Dragoset, *Phys. Rev. Lett.* **70**, 3615 (1993).

⁴¹ P. Bonanno, M. Canepa, P. Cantini, L. Mattera, R. Moroni and S. Terreni, *Surf. Sci.* **454-456**, 697 (2000).

⁴² K. Thürmer, R. Koch, M. Weber and K.H. Rieder, *Phys. Rev. Lett.* **75**, 1767 (1995).